Original Article

Oncolytic Virus Senecavirus A Inhibits Hepatocellular Carcinoma Proliferation and Growth by Inducing Cell Cycle Arrest and Apoptosis

Tao Gong[1,2#], Xiao Liu[3#], Qingyuan Li[1,2], Donald R. Branch[4], Melika Loriamini[4], Wenxian Wen[1,2], Yaoqiang Shi[2], Qi Tan[2], Bin Fan[2], Zhonghui Zhou[1], Yujia Li[2], Chunhui Yang[2], Shilin Li[2], Xiaoqiong Duan[2*] and Limin Chen[2,5,6*]

[1]Department of Clinical Medicine, North Sichuan Medical College, Nanchong, Sichuan, China; [2]Institute of Blood Transfusion, Chinese Academy of Medical Sciences and Peking Union Medical College, Chengdu, Sichuan, China; [3]College of Animal Science and Technology, Southwest University, Chongqing, China; [4]Departments of Medicine and Laboratory Medicine and Pathobiology, Centre for Innovation, Canadian Blood Services, Hamilton, Ontario, Canada; [5]The Hospital of Xidian Group, Xi'an, Shaanxi, China; [6]The Joint-Laboratory on Transfusion-Transmitted Diseases (TTDs) between Institute of Blood Transfusion and Nanning Blood Center, Nanning Blood Center, Nanning, Guangxi, China

Abstract

Background and Aims: Hepatocellular carcinoma (HCC) is a highly aggressive tumor with limited treatment options and high mortality. Senecavirus A (SVA) has shown potential in selectively targeting tumors while sparing healthy tissues. This study aimed to investigate the effects of SVA on HCC cells *in vitro* and *in vivo* and to elucidate its mechanisms of action. ***Methods:*** The cell counting kit-8 assay and colony formation assay were conducted to examine cell proliferation. Flow cytometry and nuclear staining were employed to analyze cell cycle distribution and apoptosis occurrence. A subcutaneous tumor xenograft HCC mouse model was created *in vivo* using HepG2 cells, and Ki67 expression in the tumor tissues was assessed. The terminal deoxynucleotidyl transferase dUTP nick end labeling assay and hematoxylin and eosin staining were employed to evaluate HCC apoptosis and the toxicity of SVA on mouse organs. ***Results:*** *In vitro*, SVA effectively suppressed the growth of tumor cells by inducing apoptosis and cell cycle arrest. However, it did not have a notable effect on normal hepatocytes (MIHA cells). In an *in vivo* setting, SVA effectively suppressed the growth of HCC in a mouse model. SVA treatment resulted in a significant decrease in Ki67 expression and an increase in apoptosis of tumor cells. No notable histopathological alterations were observed in the organs of mice during SVA administration. ***Conclusions:*** SVA inhibits the growth of HCC cells by inducing cell cycle arrest and apoptosis. It does not cause any noticeable toxicity to vital organs.

Citation of this article: Gong T, Liu X, Li Q, Branch DR, Loriamini M, Wen W, *et al*. Oncolytic Virus Senecavirus A Inhibits Hepatocellular Carcinoma Proliferation and Growth by Inducing Cell Cycle Arrest and Apoptosis. J Clin Transl Hepatol 2024. doi: 10.14218/JCTH.2024.00125.

Introduction

Primary liver cancer (PLC) is a prevalent form of cancer, ranking as the fourth most deadly tumor and the sixth most common in terms of new cases globally.[1] Hepatocellular carcinoma (HCC) accounts for around 90% of all PLC cases, with an annual incidence of 850,000 new cases.[2,3] Approximately 80% of HCC patients are diagnosed at an advanced stage due to the absence of early symptoms and rapid disease progression.[4] Although drugs like sorafenib are accessible, the five-year survival rate for patients with advanced liver cancer remains below 5%.[5,6] Consequently, it is crucial and of great significance to investigate novel treatment alternatives for HCC.

Oncolytic viruses (OVs) are viral agents that specifically target and eliminate cancer cells while sparing healthy tissues.[7] OVs encompass both naturally occurring and genetically engineered viruses, with the latter showing enhanced efficacy and improved targeting capabilities.[8] OVs can reproduce within tumor cells, generating additional offspring virions that destroy neighboring tumor cells through various mechanisms, including direct lysis of tumor cells, stimulation of local or systemic immune responses against the tumor, and modification of the tumor microenvironment.[9] Several studies have demonstrated significant antitumor effects of oncolytic vaccinia virus containing *Aphrocallistes vastus* lectin in HCC cells and mouse models with transplanted human tumors.[10,11] Additionally, the wild-type Newcastle disease virus HK84 strain has been reported to specifically suppress HCC, with its anticancer activity linked to the activation of

interferon (IFN) type I.[12]

Senecavirus A (SVA) is a natural oncolytic virus.[13] It is a non-segmented RNA virus with a single positive-stranded genome and lacks a vesicle membrane. SVA belongs to the genus Senecavirus within the Picornaviridae family.[14] The viral particles exhibit a characteristic symmetrical icosahedral shape, measuring approximately 27 nm in diameter and weighing around 30 kDa.[15] In 2015, the International Committee on Taxonomy of Viruses renamed the original strain of Seneca Valley virus (SVV), known as SVV-001, to SVA. Since SVA reproduces using RNA intermediates and does not go through a DNA stage or integrate into the host genome, it is considered relatively safe. Research indicates that SVA has a strong capability to target tumors with neuroendocrine characteristics.[8] A solitary intravenous administration of the oncolytic picornavirus SVV-001 eradicated medulloblastomas in primary tumor-derived orthotopic xenograft mouse models.[16] Surprisingly, the administration of 10^{14} vp/kg of the oncolytic virus SVV-001 successfully eradicated tumors in two out of six heterotransplant mouse models of a specific small cell lung cancer variant, with long-lasting effects.[17] Nevertheless, there have been no documented studies on the potential application of SVA for treating HCC.

The objective of this study was to examine the therapeutic impact of SVA on HCC through both *in vitro* and *in vivo* experiments. The MIHA cell line, a normal immortalized human hepatocyte cell line, was utilized as a normal control in the study.[18] Our investigation revealed that SVA suppresses the growth of HepG2 cells by triggering apoptosis and halting the cell cycle. Administering SVA through direct injection into the tumor effectively suppresses HCC growth in a mouse model while maintaining a favorable safety profile. The results indicate that SVA has the potential to be a new and effective treatment approach for HCC.

Methods

Cells and virus

Hepatocellular carcinoma cell line HepG2 was cryopreserved in our laboratory. The MIHA cell line, a normal immortalized human hepatocyte cell line, was generously provided by Professor Juan Chen from Chongqing Medical University, China, and used as a normal control. The BHK-21 (baby hamster kidney cells) and SVA (GenBank: MH716015.1) were acquired as a generous donation from Professor Xiao Liu of Southwest University, China. BHK-21, MIHA, and HepG2 cells were cultivated in Dulbecco's modified Eagle's medium (DMEM) from VivaCell, China, supplemented with 1% mycoplasma inhibitor from Trans, China, and 10% (V/V) fetal bovine serum (FBS) from Biological Industries, Israel. The cells were cultured in a cell incubator at 37°C with 5% CO$_2$ concentration.

Virus amplification and purification

BHK-21 cells were seeded in 10 cm culture dishes until they reached approximately 80% coverage, then the medium was replaced with 10 mL of serum-free medium. The SVA virus stock was introduced and incubated for 4 h at 37°C to facilitate virus adsorption. Subsequently, FBS was introduced to achieve a final concentration of 2%. When over 80% of the cells displayed cytopathic effects, the virus was collected by subjecting the cells to two cycles of freezing and thawing, followed by centrifugation at 12,000 ×g for 30 m to remove solid particles. The supernatant was then centrifuged at 120,000 ×g for 2 h at 4°C to concentrate it. The precipitate was resuspended in phosphate-buffered saline (PBS) to a fi-

nal volume that was 2% of the original supernatant volume. The viral suspension was then aliquoted and stored at −80°C until needed.

TCID$_{50}$ assay

Viral titers were determined by TCID$_{50}$ assays as previously described.[19] HepG2 cells were distributed at a density of 1×10^4 cells per well in a 96-well plate with DMEM supplemented with 10% FBS. Following the attachment of cells, the virus stock was diluted in serum-free DMEM from 10^{-1} to 10^{-10} in serial steps. The diluted virus was then applied to the cells for 4 h, with eight replicates for each dilution. Subsequently, the inoculum was substituted with 200 µL of DMEM supplemented with 2% FBS. Cellular morphology was observed daily to document the number of cytopathic effects. The TCID$_{50}$ (tissue culture infectious dose 50) was determined using the Reed-Muench method.[20]

Cell viability assay

HepG2 and MIHA cells were distributed in a 96-well plate at densities of 2×10^3 and 3×10^3 cells per well, respectively. The cells were subjected to SVA at specific multiplicities of infection (MOI) as specified in various assays for 4 h at 37°C. After adsorption, the medium was replaced with 200 µL of DMEM containing 10% FBS. The cells were then incubated for 24, 48, and 72 h, with three replicates for each time point. The CCK-8 assay, using the Biosharp kit from China, was conducted following the methodology previously outlined.[21] In summary, a combination of 100 µL of serum-free medium and 10 µL of CCK-8 reagent was introduced into each well. Following a 2-h incubation period at 37°C protected from light, the absorbance at a wavelength of 450 nm was quantified using a spectrophotometer from PerkinElmer, United States. Cell viability was calculated using the following formula:

$$\text{Cell survival rate (\%)} = \frac{\text{OD}_{\text{experiment}} - \text{OD}_{\text{blank}}}{\text{OD}_{\text{control}} - \text{OD}_{\text{blank}}} \times 100\%.$$

Colony formation assay

HepG2 and MIHA cells were placed in a 6-well plate at densities of 1×10^3 and 2×10^3 cells per well, respectively. The cells were exposed to either PBS or SVA at a MOI of 0.1 or 0.5. They were cultured until each clone contained more than 50 cells (two weeks). The cells were then fixed with 4% paraformaldehyde (Solarbio, China) for 30 m, stained with 0.1% crystal violet (Solarbio, China) for 15 m at room temperature, and imaged.[22] Colonies were quantified using ImageJ software.

Cell cycle analysis

Cells were infected with SVA for 24 h. The cell cycle distribution was determined using the DNA Content Quantitation Assay kit (Cell Cycle) from Solarbio, China, following the previously described method.[23] Specifically, 1 million cells were collected and preserved in pre-cooled 70% ethanol for 4 h at 4°C. The cells were then exposed to 100 µL of RNase A at 37°C for 30 m. Afterward, 400 µL of PI staining solution was added. The mixture was incubated at 4°C for 30 m in the dark and analyzed using flow cytometry (FACSCanto™, BD, USA). The data were analyzed with FlowJo software.

Detection of apoptotic cells by flow cytometry

The evaluation of apoptosis was conducted via the implementation of Annexin V/PI double staining, utilizing an Annexin

V-fluorescein (FITC)/PI apoptosis kit (BD, USA) as previously described.[24] The cells were cultured and exposed to SVA for a duration of 24 h. A total of 500,000 cells were collected, and five microliters of Annexin V and five microliters of PI staining solution were introduced. Subsequently, the cells were placed in a dark environment and maintained at room temperature for a period of 30 m. The mixture underwent flow cytometry to evaluate cell apoptosis. The data were subsequently processed using the FlowJo software. The different quadrants in the flow cytometry analysis are defined as follows: Annexin V-FITC (−)/PI (+), indicating the number of deceased cells; Annexin V-FITC (+)/PI (+), representing the number of cells in the late apoptotic/necrotic state; Annexin V-FITC (+)/PI (−), signifying the number of cells in the early apoptotic state; and Annexin V-FITC (−)/PI (−), indicating the quantity of viable cells.

Nuclear staining by Hoechst 33258

The identification of altered nuclear morphology and apoptotic body formation was conducted via Hoechst 33258 staining, in accordance with the previously described method.[25] The cells were cultured and exposed to SVA for a duration of 24 h, after which they were fixed for 30 m using 4% paraformaldehyde fixative (Solarbio, China) at room temperature. Subsequently, the cells were exposed to Hoechst 33258 staining solution (Solarbio, China) and incubated for 30 m at 37°C in the dark. Following two washes with PBS, the nuclei stained with Hoechst 33258 were visualized using an inverted fluorescence microscope manufactured by Olympus in Japan. Apoptotic cells exhibit a number of distinctive characteristics, including nuclear condensation, fragmentation, the formation of apoptotic bodies, and an increased fluorescence intensity.

Mitochondrial membrane potential (MMP) assay

The cells were infected with SVA for a duration of 24 h. The MMP was measured using a mitochondrial membrane potential assay kit with JC-1 (Beyotime, China), as previously described.[26] In conclusion, a total of one million cells were gathered and subjected to centrifugation at a speed of 1,000 revolutions per minute for a duration of 5 m. The cell precipitate should be retrieved and a 500 µL solution of JC-1 staining (20 µg/mL) should be applied to it. The mixture should be incubated at a temperature of 37°C in a light-free environment for a duration of 20 m. Subsequently, the cells underwent two washes with the JC-1 staining buffer prior to being subjected to flow cytometry analysis. The data were analyzed using the FlowJo software.

In vivo xenograft tumor model

Male BALB/c nude mice, aged four to six weeks and weighing 18–21 g, were purchased from Chengdu Ensiweier Biotechnology Co., Ltd. HepG2 cells in the logarithmic growth phase were harvested and diluted to a concentration of 5×10^7 cells per milliliter. Then, 0.1 mL of the cell suspension was injected subcutaneously into the right flank of each nude mouse. The length (a) and width (b) of the tumors were measured daily to calculate their volume using the formula: $V=(a \times b^2)/2$.[27] After the tumors grew to approximately 100 mm³, the mice were randomly divided into three groups: the PBS-treated group (100 µL/day), the SVA-treated group (6×10^6 TCID$_{50}$/day), and the cisplatin (DDP)-treated group (20 mg/kg per day). Each group consisted of 12 mice. The DDP-treated group served as a positive control to assess the antitumor effect. Each mouse received a total of three injections on alternate days directly into the tumor. After twenty-eight days following the initial treatment, the mice were euthanized, and samples of their liver, heart, spleen, lungs, kidneys, blood, and tumors were collected.

RNA isolation and RT-qPCR

Total RNA was isolated from the mouse viscera, tumor tissues, and blood using TRIzol (Invitrogen, USA), as previously described.[28] The synthesis of complementary DNAs was performed using a complementary DNA synthesis kit from Toyobo, Japan, following the manufacturer's protocol. RT-qPCR analyses were conducted using NovoStart® SYBR qPCR SuperMix Plus (Novoprotein, China), following the manufacturer's protocol. The SVA primers used were: Forward primer sequence: 5'-ATTGGTGTGGTCTGCGAGTT-3', Reverse primer sequence: 5'-GTGCGAGGGCTAAGTCTTGT-3'. The GAPDH primers used were: Forward primer sequence: 5'-GCCTCCTGCACCACCAACTG-3', Reverse primer sequence: 5'-ACGCCTGCTTCACCACCTTC-3'. The Ki67 primers used were: Forward primer sequence: 5'-ACGCCTGGTTAC-TATCAAAAGG-3', Reverse primer sequence: 5'-CAGACC-CATTTACTTGTGTTGGA-3'. The expression of Ki67 mRNA was standardized to the housekeeping gene GAPDH.

H&E staining

H&E staining was performed as previously described.[29] The visceral tissues of mice were immersed in a 4% solution of paraformaldehyde for 24 h to preserve them. After that, the tissue sections underwent dewaxing using xylene, followed by hydration with a gradient of ethanol. Subsequently, hematoxylin staining (Biosharp, China) was applied for 5 m, followed by differentiation with 1% hydrochloric acid. After counterstaining with eosin (Biosharp, China) for 3 m, the sections were dehydrated and permeabilized. After sealing with neutral resin, they were observed under an optical microscope (Leica, Germany) at 400× magnification.

Immunohistochemistry

Immunohistochemistry was performed as described previously.[30] The tumor tissues underwent fixation, dehydration, embedding, and sectioning, following the protocol outlined in the H&E staining assay mentioned earlier. The sections embedded in paraffin were dewaxed in a sequential manner. The Tris-EDTA antigen retrieval buffer from Servicebio, China, was utilized for antigen retrieval. The endogenous peroxidase activity was inhibited using a 3% solution of hydrogen peroxide obtained from the National Medicine Group in China for 25 m at room temperature in the dark. Non-specific binding was inhibited by treating with 5% normal goat serum (Solarbio, China) for 30 m at room temperature. Afterward, the sections were treated with rabbit polyclonal to Ki67 primary antibody (Abcam, UK) at 4°C overnight, followed by incubation with goat anti-rabbit secondary antibody (Servicebio, China) for 50 m at room temperature. The sections were stained with 3,3'-diaminobenzidine (Biosharp, China). Hematoxylin (Servicebio, China) was used to counterstain the cell nuclei for 30 s, and a neutral mounting medium was used for sealing. Microscopic images were acquired, and data analysis was conducted using ImageJ software.

TUNEL assay in tumor tissues

The tumor tissues underwent fixation, dehydration, embedding, and sectioning, in accordance with the protocol outlined in the H&E staining assay previously described. The detection of apoptosis was performed using an FITC TUNEL cell apoptosis detection kit (Servicebio, China), following the previously described method.[31] In conclusion, the paraffin sections were

subjected to a process of paraffin removal and proteinase K (Servicebio, China) treatment for 20 m at room temperature, which renders the sections permeable. Subsequently, the sections were incubated with TdT incubation buffer (recombinant TdT enzyme, FITC-12-dUTP Labeling Mix: Equilibration Buff=1:5:50) for 1 h at 37°C. Following this, the sections were stained with DAPI (Biosharp, China) for 10 m at room temperature in the dark. Cells that exhibited TUNEL positivity, as indicated by the presence of green nuclei, were visualized using an inverted fluorescence microscope. The data were analyzed using the ImageJ software.

Statistical analysis

The statistical analyses were conducted using GraphPad Prism version 8 software, developed by GraphPad Software in the United States. The results are presented as the mean value plus or minus the standard error of the mean. To evaluate the statistical significance of differences between the two groups, an unpaired two-tailed Student's t-test was employed. The statistical significance of the results was determined using one-way ANOVA for three or more groups. A significance level of $p < 0.05$ was employed to determine statistical significance.

Results

SVA suppresses the growth of HepG2 cells in vitro

To assess the influence of SVA on cell viability, we conducted a CCK-8 assay on HepG2 and MIHA cells, both with and without SVA infection. HepG2 and MIHA cells were exposed to SVA at three different MOIs – 0.1, 0.5, and 2.5 – for a duration of 48 h. The viability of HepG2 cells was found to have decreased significantly when compared to the control group treated with PBS. The viability of the HepG2 cells decreased significantly from 100.1±2.3% to 54.9±2.7% at MOI=0.1, 33±0.98% at MOI=0.5, and 14.3±1.45% at MOI=2.5 (Fig. 1A). Furthermore, HepG2 and MIHA cells were exposed to SVA at an MOI of 0.5, and cell viability was measured at 24 h, 48 h, and 72 h, respectively. A significant decrease in cell viability was observed over time in HepG2 cells. The viability of the HepG2 cells decreased from 100±0.6% to 73.5±2.6% at 24 h, 32.8±1.7% at 48 h, and 17.4±0.5% at 72 h. In contrast, there were no notable alterations in the survival of MIHA cells treated with SVA compared to the control group treated with PBS (Fig. 1B).

To validate the inhibitory impact of SVA on HCC cells, we conducted a colony formation assay. The number of clones formed by HepG2 cells significantly decreased from 152±2 to 46±6 and 27±6 after SVA infection at MOI of 0.1 and 0.5, respectively, in comparison to the control group treated with PBS. However, there were no notable alterations in the number of colonies produced by MIHA cells, regardless of whether they were infected with SVA or not (Fig. 1C, D). The results suggest that SVA specifically inhibits the proliferation of HCC cells.

SVA-induced cell cycle arrest at the S phase in HepG2 cells

Subsequently, we employed flow cytometry to examine the influence of SVA infection on the cell cycle advancement of HepG2 and MIHA cells that were infected with SVA. The percentage of HepG2 cells in the G0/G1 phase exhibited a significant decline from 68.3±0.5% to 62±0.6% and 53±0.4% following SVA infection at MOIs of 0.1 and 0.5, respectively, compared to the control group treated with PBS. Conversely, the percentage of HepG2 cells in the S phase increased

from 24.1±0.2% to 32.8±1.1% (MOI=0.1) and 44.9±2.8% (MOI=0.5) (Fig. 2A, B). Nevertheless, the cell cycle distribution of MIHA cells did not exhibit any notable alterations following SVA infection (Fig. 2A, C). The results demonstrate that SVA induced the HepG2 cells to cease their cell cycle at the S phase.

SVA induced apoptosis in HepG2 cells

In order to examine the influence of SVA infection on apoptosis in HCC cells, we utilized Hoechst 33258 staining to label the nuclei of HepG2 and MIHA cells following SVA infection. Subsequently, the stained cells were observed using an inverted fluorescence microscope. HepG2 cells infected with SVA exhibited typical apoptotic nuclear morphology, characterized by nuclear condensation, fragmentation, formation of apoptotic bodies, and increased fluorescence intensity, in comparison to the control group treated with PBS. The fluorescence intensity of the nuclei in MIHA cells was not significantly altered in the absence or presence of SVA infection (Fig. 3A). The findings demonstrated that SVA stimulated apoptosis in HepG2 cells.

Flow cytometry was employed to quantitatively analyze apoptosis in HepG2 and MIHA cells following SVA infection. The apoptosis rates of HepG2 cells were significantly elevated in the SVA-infected group compared to the control group treated with PBS. The rates of early and late apoptosis in HepG2 cells were 6.6±0.5% and 7.7±0.5%, respectively, when infected with SVA at a MOI of 0.1. At a MOI of 0.5, the rates of early and late apoptosis were 13.3±0.8% and 9.3±0.2%, respectively (Fig. 3B, C). Nevertheless, no significant differences were observed in the rates of apoptosis between the MIHA cells and the control group treated with PBS (Fig. 3B, D). The results indicate that SVA induces apoptosis in HepG2 cells in a manner that is dependent on dosage. However, no similar effect was observed in MIHA cells.

JC-1 is a fluorescent dye that exhibits both lipophilic and cationic properties. JC-1 exists in two distinct forms: as individual molecules, referred to as monomers, or as larger structures, known as aggregates. In the absence of pathological conditions, JC-1 molecules aggregate within the mitochondria of healthy cells, resulting in the emission of red fluorescence that can be observed using the PI channel of a flow cytometer. During apoptosis, the reduction of MMP results in heightened permeability and subsequent liberation of JC-1 from the mitochondria, where it undergoes a transition to its monomeric state. The monomeric form of JC-1 can be identified by its green fluorescence when using the FITC channel of a flow cytometer. The ratio of green to red fluorescence in cells can be used to evaluate changes in MMP, which is regarded as one of the initial biological changes in cell apoptosis. The study revealed a notable rise in the ratio of green and red fluorescence in HepG2 cells, increasing from 5.6±1% to 19.4±3% and 22.9±2.7% following SVA infection at MOIs of 0.1 and 0.5, respectively (Fig. 4A, B). The presence of SVA during incubation did not result in any noticeable variation in MMP levels in MIHA cells (Fig. 4A, C). The results indicate that SVA induced apoptosis in HepG2 cells in a manner that depended on the dosage, while it had no impact on MIHA cells.

SVA inhibited HCC cells growth in vivo

In order to examine the potential suppressive impact of SVA on the growth of HepG2 cells in living organisms, a model of subcutaneous tumor xenografts in BALB/c nude mice was created (Fig. 5A). The PBS treatment served as the negative control, while the DDP treatment served as the positive control. One mouse in the group treated with PBS died fol-
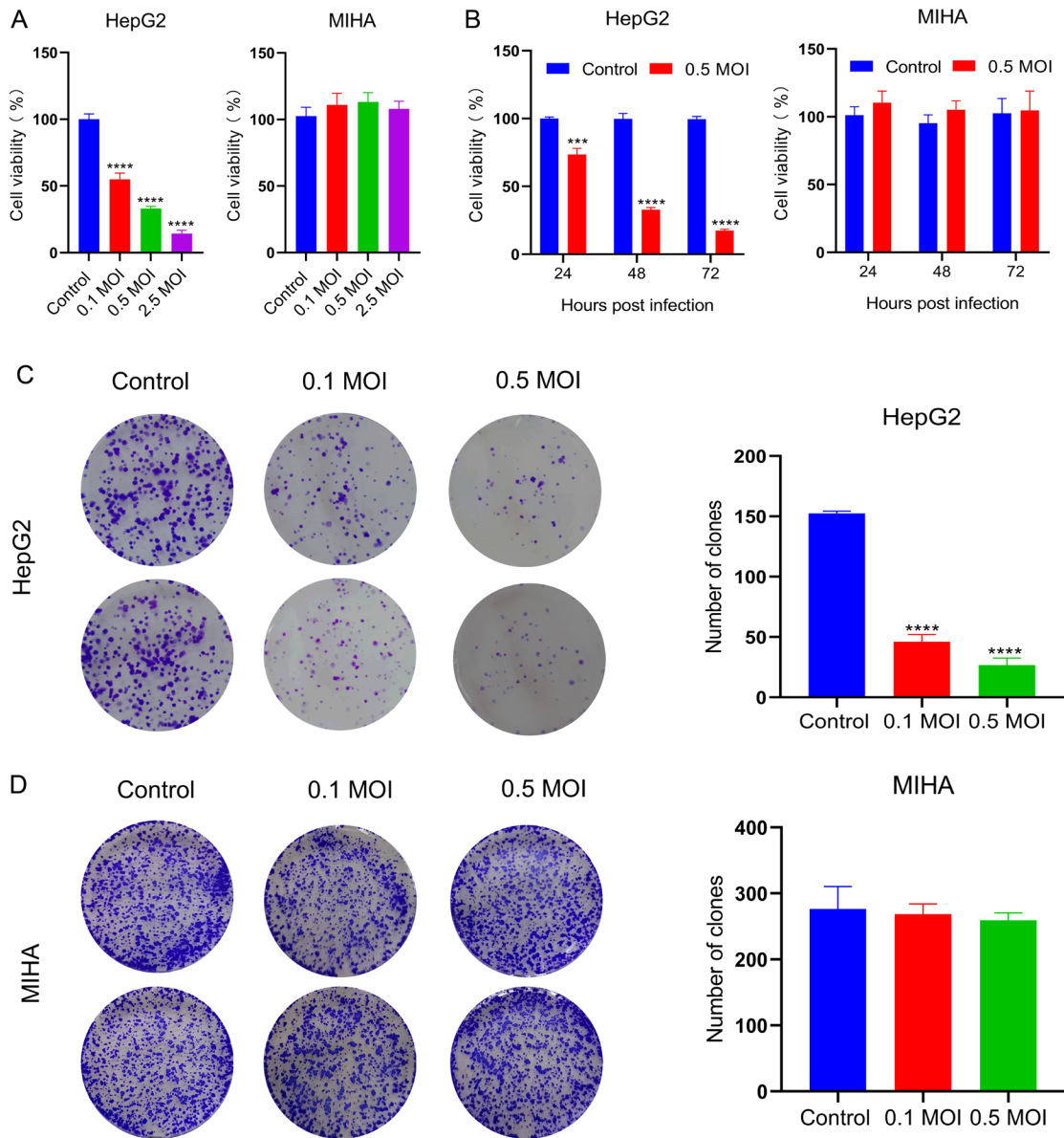
Fig. 1. Senecavirus A (SVA) inhibits the proliferation of HepG2 cells *in vitro*. (A) HepG2 and MIHA cells were exposed to either PBS or SVA (at a multiplicity of infection of 0.1, 0.5, and 2.5) for a duration of 48 h. The viability of the cells was assessed using the CCK-8 assay. The viability of HepG2 cells decreased significantly as the doses of SVA increased. (B) HepG2 and MIHA cells were exposed to either PBS or SVA (at a MOI of 0.5) for 24, 48, and 72 h. The viability of the cells was assessed using the CCK-8 assay. The application of SVA treatment led to a substantial reduction in the viability of HepG2 cells. (C and D) HepG2 and MIHA cells were exposed to either PBS or SVA (at a MOI of 0.1 or 0.5) until each clone had a cell count exceeding 50. The cells were treated with 4% paraformaldehyde for 30 m to immobilize them, followed by staining with 0.1% crystal violet for 15 m. The quantification of clones was performed using the ImageJ software. The number of clones formed by HepG2 cells was significantly decreased after SVA infection in comparison to the control group. ***$p<0.001$; ****$p<0.0001$. MIHA, immortalized hepatocyte line; MOI, multiplicities of infection; PBS, phosphate-buffered saline.

lowing the second injection. The tumor growth was significantly suppressed in both the SVA- and DDP-treated groups compared to the PBS-treated group (Fig. 5B). On day 28 following the initial injection, the tumor volumes of the groups that received PBS, SVA, and DDP were 1,330±80.6 mm^3, 808.9±102.2 mm^3, and 672.6±88.7 mm^3, respectively (Fig. 5C). The weights of eight tumors from each group were measured and recorded as follows: 0.9±0.07 g, 0.52±0.05 g, and 0.42±0.05 g (Fig. 5D). The results demonstrated that SVA effectively suppressed the proliferation of HepG2 cells in an *in vivo* setting.

Furthermore, the TUNEL assay was employed to evaluate apoptosis in tumor tissues from both the SVA-treated and PBS-treated groups. The SVA-treated group exhibited approximately double the number of TUNEL-positive cells in the tumor tissue compared to the PBS-treated group, suggesting an increase in apoptosis (Fig. 5E). Moreover, the SVA-treated group exhibited a reduction of approximately 50% in the expression of Ki67, a prominent indicator of tumor proliferation, at both the mRNA and protein levels (Fig. 5F, G, respectively). These findings indicate that SVA suppresses the growth of HepG2 cells in living organisms, most likely by
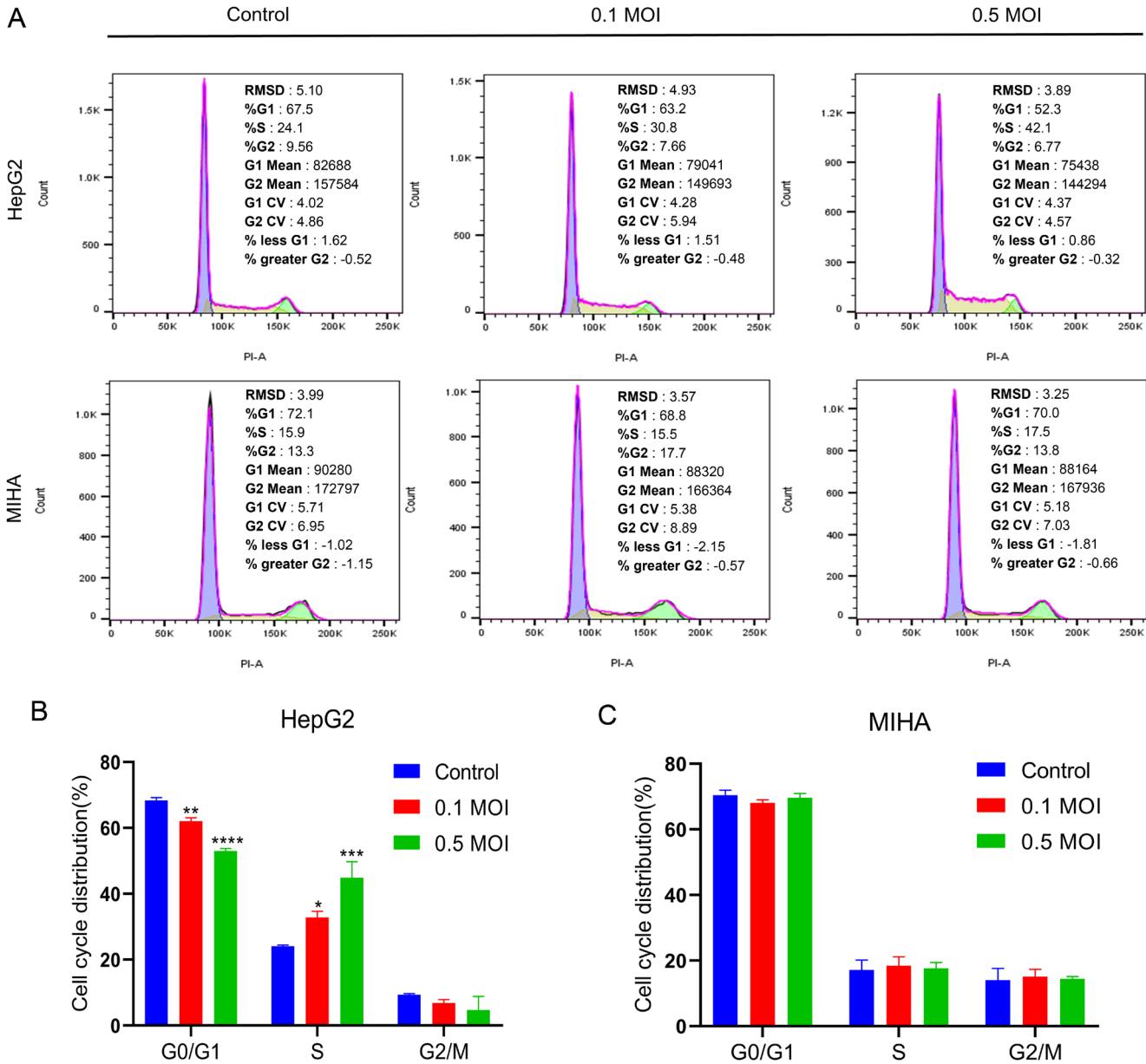
Fig. 2. Senecavirus A (SVA) induced cell cycle arrest in HepG2 cells at the S phase. HepG2 and MIHA cells were subjected to treatment with either PBS or SVA at a multiplicity of infection (MOI) of 0.1 or 0.5 for a duration of 24 h. The distribution of the cell cycle was assessed through flow cytometry following treatment with 100 µL of RNase A and 400 µL of PI staining solution. The data is displayed as the average±standard error of the mean (n=3), *p<0.05; **p<0.01; ***p<0.001; ****p<0.001. (A) The SVA infection markedly decreased the percentage of HepG2 cells in the G0/G1 phase and increased the percentage of HepG2 cells in the S phase. (B and C) Quantitative analysis of flow cytometry data. MIHA, immortalized hepatocyte line; RMSD, root mean square deviation.

enhancing programmed cell death.

Toxicity analysis of SVA in mice

In order to assess the toxicity of SVA on mice, we initially quantified the levels of SVA RNA in various tissues, including the liver, heart, spleen, lung, kidney, blood, and tumor samples obtained from the mice at the end of the experiment. The presence of SVA RNA was exclusively observed in the liver, tumor tissue, and blood of the SVA-treated mice. Conversely, no SVA RNA was detected in the heart, spleen, lung, and kidney (Fig. 6A). The level of SVA RNA in tumor tissue was significantly higher than that observed in the

mouse liver. The histological examination of mouse heart, liver, spleen, lung, and kidney tissues revealed no notable pathological alterations when compared to the PBS-treated group, as indicated by H&E staining (Fig. 6B). These findings indicate that direct delivery of SVA into the tumor is a secure and efficacious approach for the treatment of HCC.

Discussion

SVV-001, an oncolytic picornavirus that occurs naturally, was initially discovered in 2002 in a cell culture that was likely contaminated with porcine trypsin or bovine serum contain-
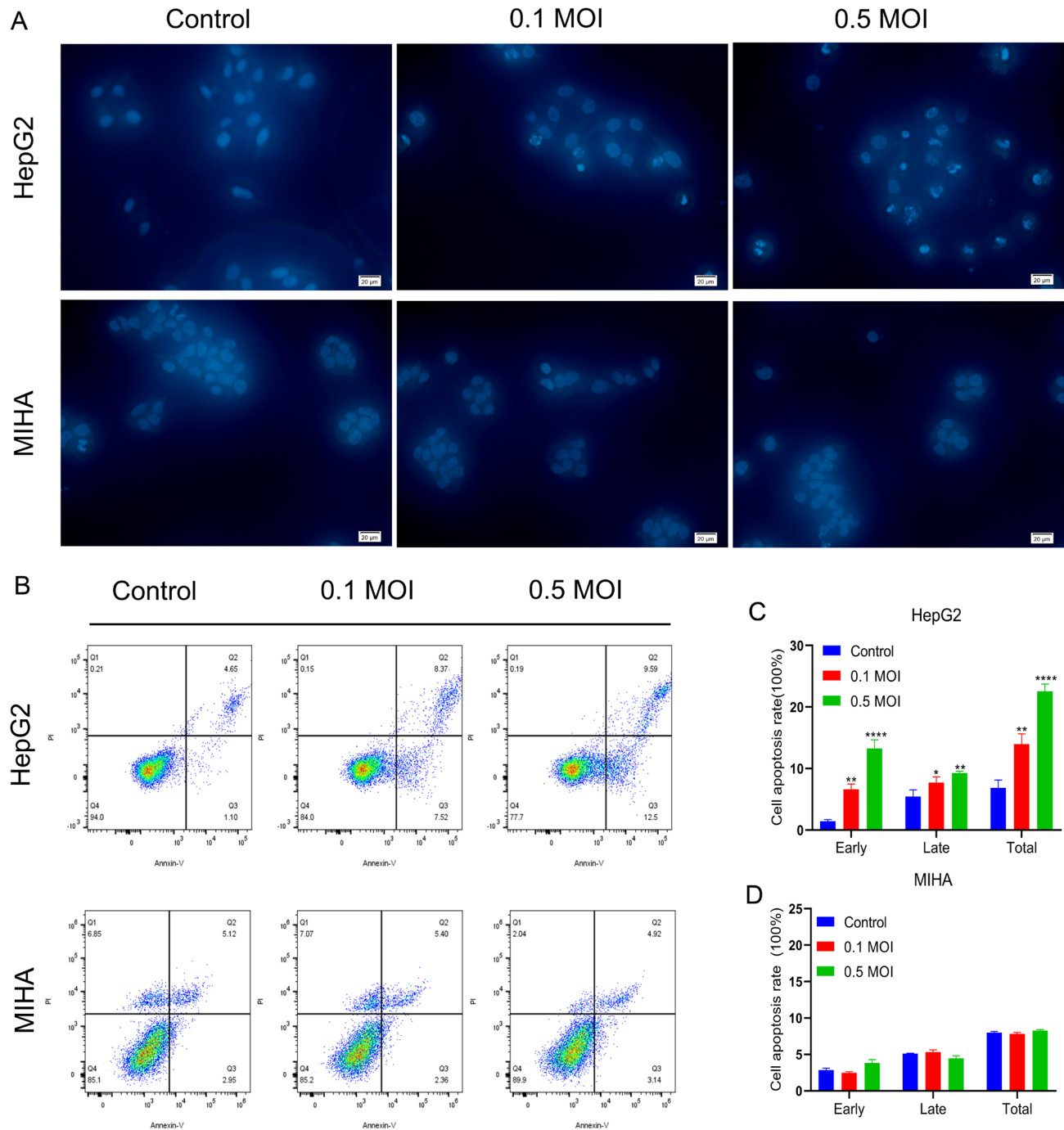
Fig. 3. Senecavirus A (SVA) induced apoptosis in HepG2 cells. HepG2 and MIHA cells were exposed to either PBS or SVA (at a multiplicity of infection of 0.1 or 0.5) for a duration of 24 h. The data are displayed as the average value plus or minus the standard error of the mean (SEM). *$p<0.05$; **$p<0.01$; ****$p<0.0001$. (A) HepG2 and MIHA cells were subjected to Hoechst 33258 staining for a duration of 30 m, followed by examination of their nuclear morphology using an inverted fluorescence microscope. The SVA infection prominently triggered nuclear condensation, fragmentation, and the formation of apoptotic bodies in HepG2 cells. Additionally, it led to an increase in fluorescence intensity. (B) The HepG2 and MIHA cells were subjected to staining using Annexin V and PI staining solution. Flow cytometry was employed to quantify apoptosis. The infection of SVA markedly elevated the apoptosis rates of HepG2 cells. (C and D) Quantitative analysis and visualization of data obtained from flow cytometry. MIHA, immortalized hepatocyte line; MOI, multiplicities of infection.

ing SVV-001.[32] SVV-001 has been proven to exhibit specific cytotoxicity towards tumor cells that exhibit neuroendocrine characteristics.[32] In this study, we sought to examine the impact of SVA on HCC cells. Notably, this study represented the first demonstration of SVA's strong oncolytic activity against HepG2 cells in both laboratory settings and live organisms. It is of note that SVA does not cause any harm to normal human liver cells or mouse organs.
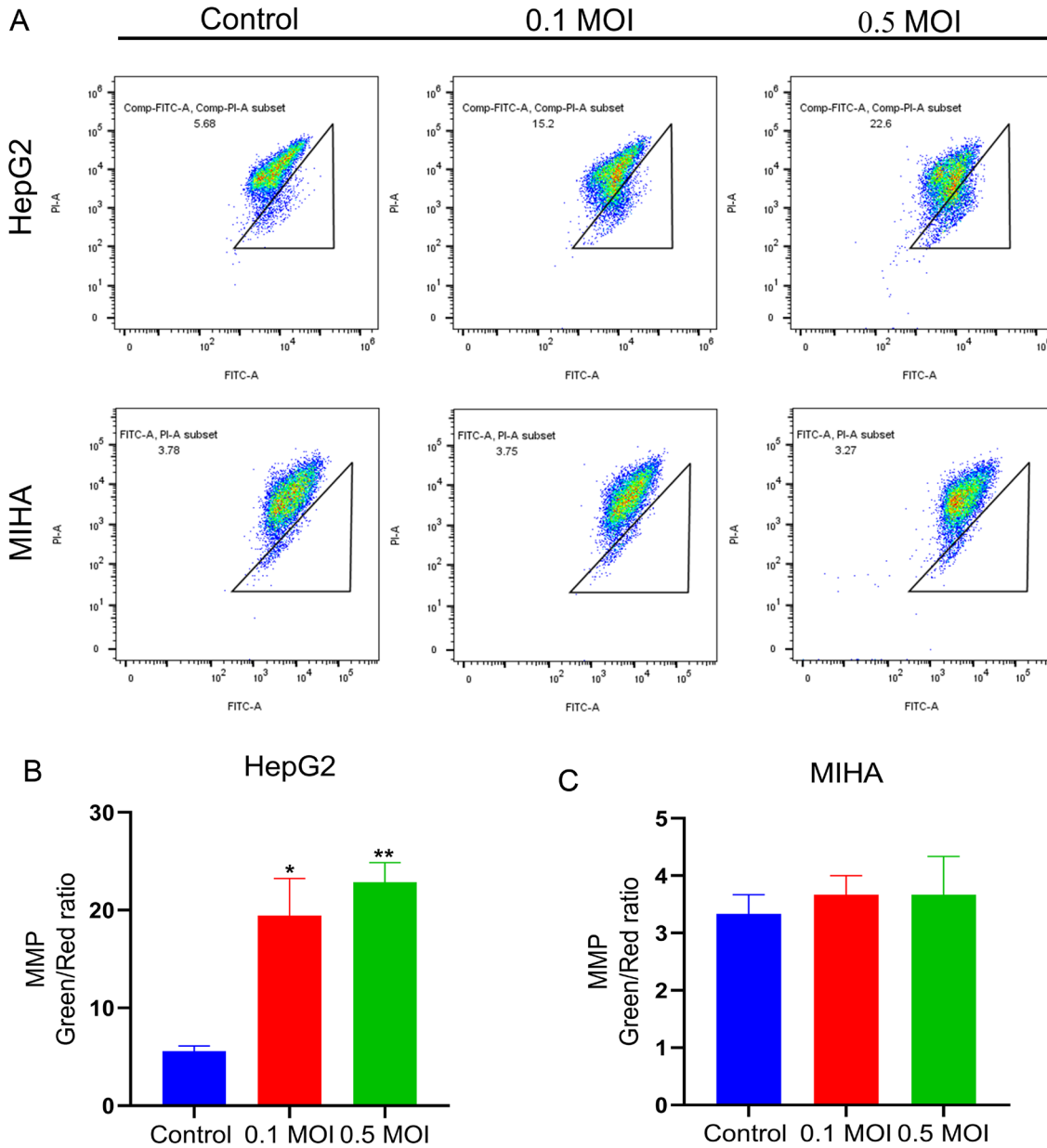
Fig. 4. Senecavirus A (SVA) decreases the MMP of HepG2 cells. HepG2 and MIHA cells were exposed to either PBS or SVA (at a multiplicity of infection of 0.1 or 0.5) for a duration of 24 h. Following this, the cells were stained using JC-1 staining. The MMP was subsequently measured using flow cytometry. A greater proportion of green fluorescence relative to red fluorescence in cells signifies a decrease in mitochondrial membrane potential (MMP) and an increase in the quantity of apoptotic cells. The data is displayed as the average value plus or minus the standard error of the mean. *$p < 0.05$; **$p < 0.01$. (A) The infection of HepG2 cells with SVA significantly augmented the proportion of green and red fluorescence. (B and C) Quantitative analysis and visualization of flow cytometry data. MIHA, immortalized hepatocyte line; MOI, multiplicities of infection.

The cell cycle serves as the foundation for cell proliferation, with a primary emphasis on two key events: the duplication of genomic DNA during the S phase and its subsequent distribution into two daughter cells. In the event of a disruption to the process of DNA replication, a series of DNA repair signaling events will be initiated, resulting in the extension of the S phase.[33] A significant proportion of viruses employ the strategy of subverting the replication cycle of the host cell in order to create a cellular environment that is conducive to viral replication.[34] The nucleocapsid protein of the porcine epidemic diarrhea virus coronavirus interacts with

p53, resulting in cell cycle arrest specifically in the S phase.[35] This interaction ultimately facilitates viral replication.[35] Our study revealed that SVA infection in HepG2 cells leads to a decrease in the proportion of cells in the G0/G1 phase and an increase in the proportion of cells in the S phase. This indicated that the cell cycle is arrested and blocked, resulting in the accumulation of cells in the S phase and inhibition of cell proliferation. The inhibitory effect of SVA infection was confirmed by the decrease in HepG2 cell viability and clone formation, as well as the reduced expression of Ki67 protein in SVA-treated tumor tissues (Figs. 1 and 5F, G). The Ki67
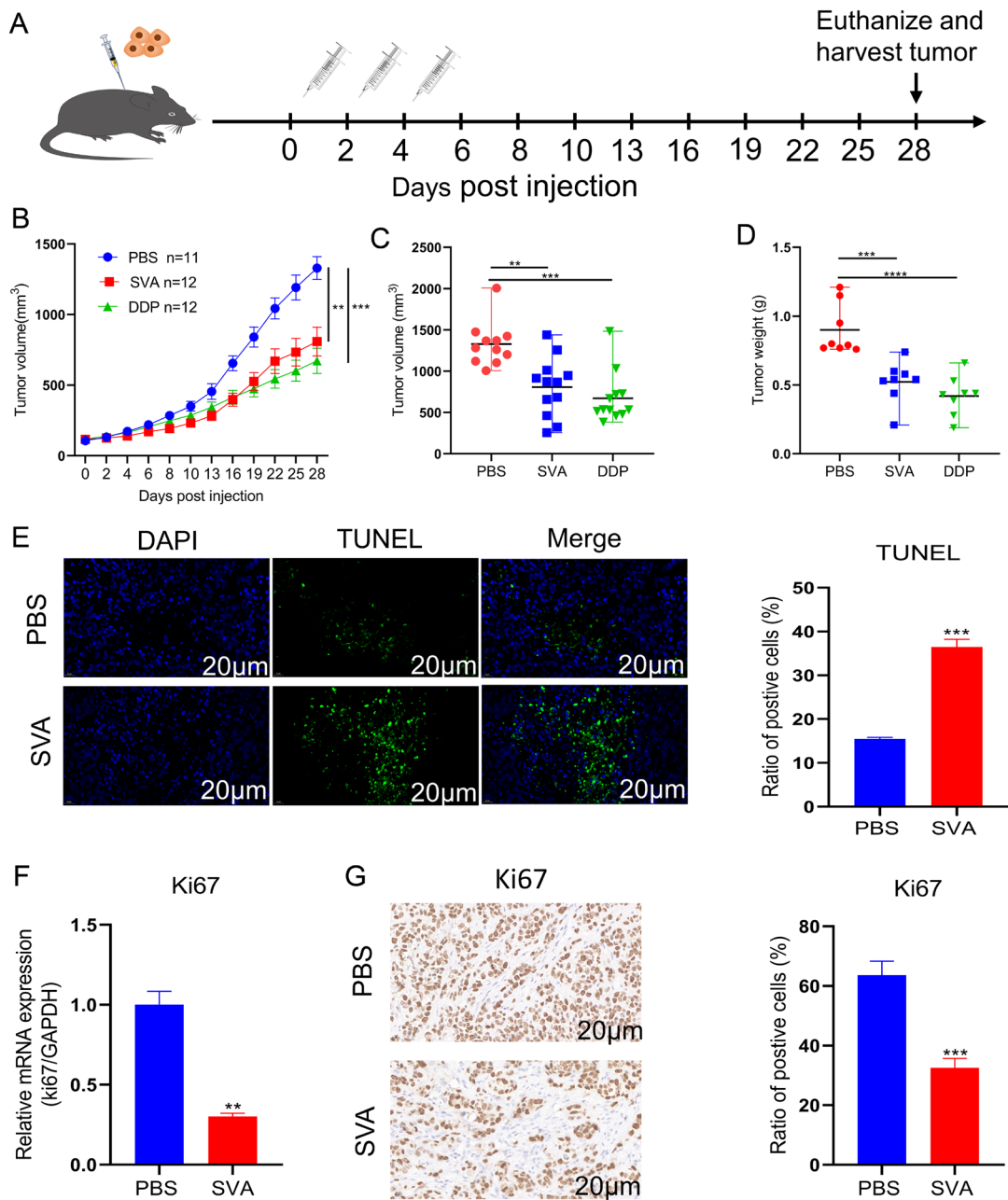
Fig. 5. Oncolytic effect of Senecavirus A (SVA) virus *in vivo*. HepG2 cells, at a concentration of 2.5×10^6 cells per site, were injected into the flanks of male BALB/c nude mice. The tumor volumes in the mice reached approximately 100 mm³ within seven days of injection. Subsequently, the mice were administered intratumorally multipoint injections of PBS (100 µL/day), SVA (6×10^6 TCID$_{50}$/day), or cisplatin (DDP) (20 mg/kg per day) on alternate days for three cycles. **$p<0.01$; ***$p<0.001$; ****$p<0.0001$. (A) Schematic diagram illustrating the process of mouse modeling and treatment. (B) Tumor volumes were assessed at three-day intervals. The tumor volume was determined by applying the formula: $V=(a\times b^2)/2$, where "a" represents the length and "b" represents the width. SVA significantly suppressed tumor growth in mice. (C and D) The measurement of tumor volumes and weights in the mice was performed. Tumors in the SVA- and DDP-treated groups showed a substantial decrease in both volume and weight compared to the PBS-treated group. (E) The terminal deoxynucleotidyl transferase dUTP nick end labeling assay (TUNEL) assay was conducted to identify apoptosis within the tumor tissues. The SVA-treated group exhibited a notable increase in the quantity of TUNEL-positive cells in tumor tissue, in contrast to the PBS-treated group. The SVA treatment effectively triggered apoptosis in HCC tissues. (F) The SVA-treated group exhibited a significant decrease in Ki67 mRNA levels. (G) Immunohistochemical analysis was conducted to assess the expression of the Ki67 protein in tumor tissues. A notable decrease in the number of Ki67-positive cells was observed in the tumor tissues of mice treated with SVA, in comparison to the group treated with PBS. PBS, phosphate-buffered saline; DDP, cisplatin; DAPI, 4',6-diamidino-2-phenylindole; FBS, fetal bovine serum.

protein is a widely recognized indicator used to evaluate cell proliferation.[36,37] It is typically found only in cells that are actively dividing. It has been documented that Ki67 plays a crucial role in the normal progression of the S phase and the arrest of the cell cycle.[38,39] Consequently, our findings indicated that SVA induced cell cycle arrest at the S phase in HepG2 cells, thereby inhibiting tumor cell proliferation. Nevertheless, it should be noted that our study is subject
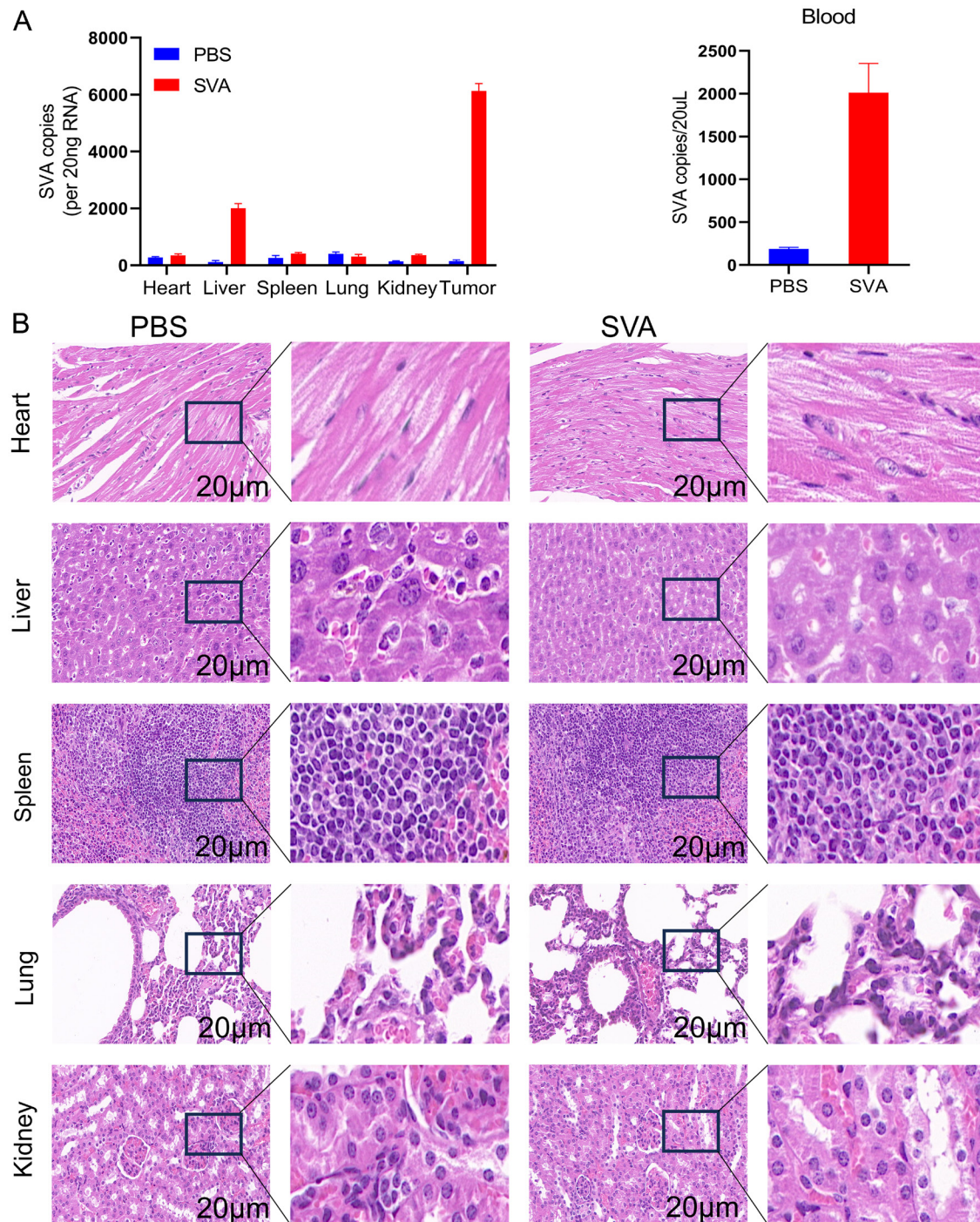
Fig. 6. Toxicity analysis of Senecavirus A (SVA) in mice. (A) The quantification of SVA RNA levels in visceral tissues, blood, and tumor tissues of the mice was performed using RT-qPCR. Following treatment, SVA can be observed in tumor tissues, the mouse liver, and the blood. (B) Hematoxylin and eosin (H&E) staining was performed to evaluate pathological alterations within the internal organs of the mice. The group of mice treated with SVA did not exhibit any notable pathological changes in the heart, liver, spleen, lungs, or kidneys. PBS, phosphate-buffered saline.

to certain limitations. Further experimentation is required to elucidate the precise signaling mechanisms involved in cell cycle arrest following SVA infection.

Furthermore, the inhibition of tumor cell proliferation was significantly correlated with the stimulation of apoptosis. Xu *et al*. provided evidence that the A-to-I edited form of miRNA-379-5p suppressed the growth of cancer cells by promoting apoptosis through CD97 activation.[40] A separate study demonstrated that methanol derived from D. linearis effectively suppressed the growth of human breast cancer cells by causing cell cycle arrest in the S-phase and promoting apoptosis.[41] Research has demonstrated that in the majority of can-

cer cases, the apoptosis process is suppressed to promote the growth of tumor cells.[42] Consequently, a significant proportion of drugs exert their anti-tumor effect by stimulating apoptosis in tumor cells.[43] Furthermore, it has been documented that SVV has the ability to trigger apoptosis in medulloblastomas.[16] SVV proteins 2C and 3Cpro were found to trigger apoptosis in tumor cells through the intrinsic pathway, which is mediated by mitochondria.[44] Moreover, Newcastle disease virus, reovirus, and vesicular stomatitis virus were found to induce apoptosis in tumor cells.[45–47] In our study, we observed that SVA had a significant inhibitory effect on the proliferation of HepG2 cells. This was evidenced by the reduced cell viability observed in the CCK-8 assay and the decreased number of cell clones in the cell clone formation assay. Furthermore, our findings demonstrated that SVA induced apoptosis, as evidenced by nuclear condensation, fragmentation, and the formation of apoptotic bodies. Additionally, SVA was found to result in a reduction in MMP. In conclusion, our findings indicate that SVA infection in HepG2 cells results in the cessation of the cell cycle and the initiation of apoptosis, thereby impeding the proliferation of tumor cells.

Ensuring the safety is a paramount consideration in the field of oncolytic virus therapy. Prior studies have indicated that in A/J mice, a breed that is susceptible to viral replication, no toxic effects that would restrict the dosage were observed following a single systemic injection of SVV-001 at doses up to 1×10^{14} vp/kg.[48] Moreover, a Phase I clinical trial of SVV-001 therapy for advanced solid tumors with neuroendocrine characteristics was conducted, administering doses ranging from 10^7 to 10^{11} vp/kg.[49] The trial demonstrated that SVV-001 treatment was safe and well-tolerated. In this study, the presence of SVA RNA was observed in the mouse liver tissues 28 days after intratumorally injections of SVA. Nevertheless, the amount of viral RNA detected was considerably lower compared to the levels found in tumors. Additionally, it was observed that in a specific mouse utilized in the experiment, the tumor completely vanished. Notably, the presence of SVA RNA in the liver tissue was no longer detectable at two weeks after the tumor disappeared (data not shown). Therefore, we hypothesized that after undergoing significant replication within the tumor, SVA may infiltrate the bloodstream and subsequently migrate to the liver. However, it is unable to replicate within the liver tissues of healthy mice. Furthermore, it is crucial to acknowledge that the mice employed in this study exhibited a weakened immune system, which might have contributed to their inability to effectively eliminate SVA. This could also account for the observable presence of SVA in the bloodstream and liver of the mice, even 28 days after the initial injection into the tumor. Consequently, further investigation is necessary to obtain additional information regarding the infection and replication of SVA in the liver of mice with a fully functioning immune system. In addition, histological examination of liver, heart, spleen, lung, and kidney tissues from mice treated with SVA revealed no discernible pathological alterations when compared to the control group treated with PBS. These results are consistent with those of previous studies.[48,49] These findings indicate that intratumorally administration of SVA treatment for HCC is a safe approach.

This study is subject to a number of limitations. Firstly, while the evidence presented in this study indicates that SVA inhibits the growth of HCC by causing cell cycle arrest and apoptosis, the specific mechanisms behind this need to be determined. Although we have confirmed that SVA causes cell apoptosis through various means, including the presence of apoptosis-related chromatin condensation, fragmentation, formation of apoptotic bodies, and increased fluorescence intensity observed using Hoechst 33258 dye, an increased proportion of apoptotic cells was detected by the Annexin V-FITC/PI apoptosis kit (FCM). Furthermore, disrupted mitochondrial membrane potential was detected by a specific detection kit (FCM) in cells, and DNA degradation in tumor tissues was observed using the TUNEL assay, it is necessary to validate additional apoptosis-related biomarkers such as caspase enzymes, cytosolic proteins, and DNA nucleosomes in the future. This will facilitate a more comprehensive comprehension of the specific mechanism by which SVA induces apoptosis. Moreover, a model of subcutaneous tumor xenograft in mice lacking immune function was created using a hepatocellular carcinoma cell line. Nevertheless, it remains unclear whether immunocompetent mice with patient-derived HCC cells will exhibit anti-tumor effects. Furthermore, the administration of SVA involved intratumoral multipoint injections. Nevertheless, it is worth exploring whether a more convenient method, such as intravenous tail injection, can be used. Although SVA injection did not result in significant pathological alterations in non-tumor tissues of mice, further research is required to determine the safety of SVA on non-tumor tissues.

Conclusion

The *in vitro* study demonstrated that SVA effectively suppressed the growth of the HCC cell line HepG2 by causing cell cycle arrest and apoptosis. Nevertheless, no analogous effects were observed in the normal liver cell line MIHA. Within a living organism, the administration of SVA effectively suppressed the growth of HCC in a mouse model placed beneath the skin by triggering apoptosis. Furthermore, we have demonstrated that intratumoral administration of SVA is not associated with any safety concerns. Collectively, the data indicate that SVA could be a promising new therapeutic approach for HCC.

Funding

Conflict of interest

LC has been an Associate Editor of the *Journal of Clinical and Translational Hepatology* since 2013. The other authors have no conflicts of interest related to this publication.

Author contributions

Project design and direction (TG, XD, XL, LC), performing the experiments and drafting the initial manuscript (TG, QL, WW), reference collection (YS, QT, BF), reviewing the initial draft (YL, ZZ, SL), manuscript revision (DRB, ML, CY, LC, XD). All authors contributed to the manuscript and approved the submitted version.

Ethical statement

This animal study protocol was approved by the ethics committee of the Institute of Blood Transfusion, Chinese Academy of Medical Sciences, and Peking Union Medical College (NO:2023023). All animals received human care.

Data sharing statement

All relevant information is provided in this current manuscript. If required, the data presented in this work can be shared via e-mail.

References

[1] Wang S, Lu Q, Ye Z, Liu F, Yang N, Pan Z, *et al*. Effects of a smartphone application named "Shared Decision Making Assistant" for informed patients with primary liver cancer in decision-making in China: a quasi-experimental study. BMC Med Inform Decis Mak 2022;22(1):145. doi:10.1186/s12911-022-01883-w, PMID:35641979.

[2] Llovet JM, Kelley RK, Villanueva A, Singal AG, Pikarsky E, Roayaie S, *et al*. Hepatocellular carcinoma. Nat Rev Dis Primers 2021;7(1):6. doi:10.1038/s41572-020-00240-3, PMID:33479024.

[3] Ghavimi S, Apfel T, Azimi H, Persaud A, Pyrsopoulos NT. Management and Treatment of Hepatocellular Carcinoma with Immunotherapy: A Review of Current and Future Options. J Clin Transl Hepatol 2020;8(2):168–176. doi:10.14218/JCTH.2020.00001, PMID:32832397.

[4] Li DP, Fan J, Wu YJ, Xie YF, Zha JM, Zhou XM. MiR-155 up-regulated by TGF-beta promotes epithelial-mesenchymal transition, invasion and metastasis of human hepatocellular carcinoma cells in vitro. Am J Transl Res 2017;9(6):2956–2965. PMID:28670383.

[5] Rodenak-Kladniew B, Castro A, Stärkel P, De Saeger C, García de Bravo M, Crespo R. Linalool induces cell cycle arrest and apoptosis in HepG2 cells through oxidative stress generation and modulation of Ras/MAPK and Akt/mTOR pathways. Life Sci 2018;199:48–59. doi:10.1016/j.lfs.2018.03.006, PMID:29510199.

[6] Baiocchi L, Francis H, Alpini G. Therapeutic Use of Viruses: Newcastle Disease Virus HK84 Oncolytic Treatment for Hepatocellular Carcinoma. J Clin Transl Hepatol 2022;10(5):783–785. doi:10.14218/JCTH.2022.00229, PMID:36304496.

[7] Yuan M, Webb E, Lemoine NR, Wang Y. CRISPR-Cas9 as a Powerful Tool for Efficient Creation of Oncolytic Viruses. Viruses 2016;8(3):72. doi:10.3390/v8030072, PMID:26959050.

[8] Muthukutty P, Yoo SY. Oncolytic Virus Engineering and Utilizations: Cancer Immunotherapy Perspective. Viruses 2023;15(8):1645. doi:10.3390/v15081645, PMID:37631987.

[9] Tian Y, Xie D, Yang L. Engineering strategies to enhance oncolytic viruses in cancer immunotherapy. Signal Transduct Target Ther 2022;7(1):117. doi:10.1038/s41392-022-00951-x, PMID:35387984.

[10] Jiang R, Qiu Y, Zhang X, Zhou N, Jia X, Chen K, *et al*. Oncolytic Vaccinia Virus Harboring Aphrocallistes vastus Lectin Inhibits the Growth of Hepatocellular Carcinoma Cells. Mar Drugs 2022;20(6):378. doi:10.3390/md20060378, PMID:35736181.

[11] Zheng X, Xu W, Ying Q, Ni J, Jia X, Zhou Y, *et al*. Oncolytic Vaccinia Virus Carrying Aphrocallistes vastus Lectin (oncoVV-AVL) Enhances Inflammatory Response in Hepatocellular Carcinoma Cells. Mar Drugs 2022;20(11):667. doi:10.3390/md20110667, PMID:36354990.

[12] Chen L, Niu Y, Sun J, Lin H, Liang G, Xiao M, *et al*. Oncolytic Activity of Wild-type Newcastle Disease Virus HK84 Against Hepatocellular Carcinoma Associated with Activation of Type I Interferon Signaling. J Clin Transl Hepatol 2022;10(2):284–296. doi:10.14218/JCTH.2021.00284, PMID:35528990.

[13] Venkataraman S, Reddy SP, Loo J, Idamakanti N, Hallenbeck PL, Reddy VS. Structure of Seneca Valley Virus-001: an oncolytic picornavirus representing a new genus. Structure 2008;16(10):1555–1561. doi:10.1016/j.str.2008.07.013, PMID:18940610.

[14] Hales LM, Knowles NJ, Reddy PS, Xu L, Hay C, Hallenbeck PL. Complete genome sequence analysis of Seneca Valley virus-001, a novel oncolytic picornavirus. J Gen Virol 2008;89(Pt 5):1265–1275. doi:10.1099/vir.0.83570-0, PMID:18420805.

[15] Dall Agnol AM, Miyabe FM, Leme RA, Oliveira TES, Headley SA, Alfieri AA, *et al*. Quantitative analysis of senecavirus A in tissue samples from naturally infected newborn piglets. Arch Virol 2018;163(2):527–531. doi:10.1007/s00705-017-3630-8, PMID:29134335.

[16] Yu L, Baxter PA, Zhao X, Liu Z, Wadhwa L, Zhang Y, *et al*. A single intravenous injection of oncolytic picornavirus SVV-001 eliminates medulloblastomas in primary tumor-based orthotopic xenograft mouse models. Neuro Oncol 2011;13(1):14–27. doi:10.1093/neuonc/noq148, PMID:21075780.

[17] Poirier JT, Dobromilskaya I, Moriarty WF, Peacock CD, Hann CL, Rudin CM. Selective tropism of Seneca Valley virus for variant subtype small cell lung cancer. J Natl Cancer Inst 2013;105(14):1059–1065. doi:10.1093/jnci/djt130, PMID:23739064.

[18] Brown JJ, Parashar B, Moshage H, Tanaka KE, Engelhardt D, Rabbani E, *et al*. A long-term hepatitis B viremia model generated by transplanting nontumorigenic immortalized human hepatocytes in Rag-2-deficient mice. Hepatology 2000;31(1):173–181. doi:10.1002/hep.510310126, PMID:10613743.

[19] Chong P, Guo MS, Lin FH, Hsiao KN, Weng SY, Chou AH, *et al*. Immunological and biochemical characterization of coxsackie virus A16 viral particles. PLoS One 2012;7(11):e49973. doi:10.1371/journal.pone.0049973, PMID:23226233.

[20] Lei C, Yang J, Hu J, Sun X. On the Calculation of TCID(50) for Quantitation of Virus Infectivity. Virol Sin 2021;36(1):141–144. doi:10.1007/s12250-020-00230-5, PMID:32458296.

[21] Qiu YB, Wan BB, Liu G, Wu YX, Chen D, Lu MD, *et al*. Nrf2 protects against seawater drowning-induced acute lung injury via inhibiting ferroptosis. Respir Res 2020;21(1):232. doi:10.1186/s12931-020-01500-2, PMID:32907551.

[22] Guo Y, Zhang Y, Cen K, Dai Y, Mai Y, Hong K. Construction and validation of a signature for T cell-positive regulators related to tumor microenvironment and heterogeneity of gastric cancer. Front Immunol 2023;14:1125203. doi:10.3389/fimmu.2023.1125203, PMID:37711621.

[23] Xu Y, Yuan H, Luo Y, Zhao YJ, Xiao JH. Ganoderic Acid D Protects Human Amniotic Mesenchymal Stem Cells against Oxidative Stress-Induced Senescence through the PERK/NRF2 Signaling Pathway. Oxid Med Cell Longev 2020;2020:8291413. doi:10.1155/2020/8291413, PMID:32774686.

[24] Mardina V, Ilyas S, Harmawan T, Halimatussakdiah H, Tanjung M. Antioxidant and cytotoxic activities of the ethyl acetate extract of Sphagneticola trilobata (L.) J.F. Pruski on MCF-7 breast cancer cell. J Adv Pharm Technol Res 2020;11(3):123–127. doi:10.4103/japtr.JAPTR_31_20, PMID:33102195.

[25] Amawi H, Hussein NA, Ashby CR Jr, Alnafisah R, Sanglard LM, Manivannan E, *et al*. Bax/Tubulin/Epithelial-Mesenchymal Pathways Determine the Efficacy of Silybin Analog HM015k in Colorectal Cancer Cell Growth and Metastasis. Front Pharmacol 2018;9:520. doi:10.3389/fphar.2018.00520, PMID:29875662.

[26] Zheng WB, Li YJ, Wang Y, Yang J, Zheng CC, Huang XH, *et al*. Propafenone suppresses esophageal cancer proliferation through inducing mitochondrial dysfunction. Am J Cancer Res 2017;7(11):2245–2256. PMID:29218248.

[27] Wedge ME, Jennings VA, Crupi MJF, Poutou J, Jamieson T, Pelin A, *et al*. Virally programmed extracellular vesicles sensitize cancer cells to oncolytic virus and small molecule therapy. Nat Commun 2022;13(1):1898. doi:10.1038/s41467-022-29526-8, PMID:35393414.

[28] Zietzer A, Hosen MR, Wang H, Goody PR, Sylvester M, Latz E, *et al*. The RNA-binding protein hnRNPU regulates the sorting of microRNA-30c-5p into large extracellular vesicles. J Extracell Vesicles 2020;9(1):1786967. doi:10.1080/20013078.2020.1786967, PMID:32944175.

[29] Hua Z, Dai S, Li S, Wang J, Peng H, Rong Y, *et al*. Deciphering the protective effect of Buzhong Yiqi Decoction on osteoporotic fracture through network pharmacology and experimental validation. J Orthop Surg Res 2023;18(1):86. doi:10.1186/s13018-023-03545-7, PMID:36737821.

[30] Ke Y, Su S, Duan C, Wang Y, Cao G, Fang Z, *et al*. Hsa_circ_0076931 suppresses malignant biological properties, down-regulates miR-6760-3p through direct binding, and up-regulates CCBE1 in glioma. Biosci Rep 2022;42(1):BSR20211895. doi:10.1042/BSR20211895, PMID:34931668.

[31] Wang W, Guan J, Feng Y, Nie L, Xu Y, Xu H, *et al*. Polystyrene microplastics induced nephrotoxicity associated with oxidative stress, inflammation, and endoplasmic reticulum stress in juvenile rats. Front Nutr 2022;9:1059660. doi:10.3389/fnut.2022.1059660, PMID:36687698.

[32] Corbett V, Hallenbeck P, Rychahou P, Chauhan A. Evolving role of seneca valley virus and its biomarker TEM8/ANTXR1 in cancer therapeutics. Front Mol Biosci 2022;9:930207. doi:10.3389/fmolb.2022.930207, PMID:36090051.

[33] Pan Z, Luo Y, Xia Y, Zhang X, Qin Y, Liu W, *et al*. Cinobufagin induces cell cycle arrest at the S phase and promotes apoptosis in nasopharyngeal carcinoma cells. Biomed Pharmacother 2020;122:109763. doi:10.1016/j.biopha.2019.109763, PMID:31918288.

[34] Wang Y, Wang R, Li Y, Sun Y, Song C, Zhan Y, *et al*. Newcastle disease virus induces G(0)/G(1) cell cycle arrest in asynchronously growing cells. Virology 2018;520:67–74. doi:10.1016/j.virol.2018.05.005, PMID:29793075.

[35] Su M, Shi D, Xing X, Qi S, Yang D, Zhang J, *et al*. Coronavirus Porcine Epidemic Diarrhea Virus Nucleocapsid Protein Interacts with p53 To Induce Cell Cycle Arrest in S-Phase and Promotes Viral Replication. J Virol 2021;95(16):e0018721. doi:10.1128/JVI.00187-21, PMID:34037422.

[36] Yang C, Zhang J, Ding M, Xu K, Li L, Mao L, *et al*. Ki67 targeted strategies for cancer therapy. Clin Transl Oncol 2018;20(5):570–575. doi:10.1007/s12094-017-1774-3, PMID:29058263.

[37] Scholzen T, Gerdes J. The Ki-67 protein: from the known and the unknown. J Cell Physiol 2000;182(3):311–322. doi:10.1002/(SICI)1097-4652(200003)182:3<311::AID-JCP1>3.0.CO;2-9, PMID:10653597.

[38] Sun X, Bizhanova A, Matheson TD, Yu J, Zhu LJ, Kaufman PD. Ki-67 Contributes to Normal Cell Cycle Progression and Inactive X Heterochromatin in p21 Checkpoint-Proficient Human Cells. Mol Cell Biol 2017;37(17):e00569–16. doi:10.1128/MCB.00569-16, PMID:28630280.

[39] Lima KG, Krause GC, da Silva EFG, Xavier LL, Martins LAM, Alice LM, *et al*. Octyl gallate reduces ATP levels and Ki67 expression leading HepG2 cells to cell cycle arrest and mitochondria-mediated apoptosis. Toxicol In Vitro 2018;48:11–25. doi:10.1016/j.tiv.2017.12.017, PMID:29288082.

[40] Xu X, Wang Y, Mojumdar K, Zhou Z, Jeong KJ, Mangala LS, *et al*. A-to-I-edited miRNA-379-5p inhibits cancer cell proliferation through CD97-induced apoptosis. J Clin Invest 2019;129(12):5343–5356. doi:10.1172/JCI123396, PMID:31682236.

[41] Baharuddin AA, Roosli RAJ, Zakaria ZA, Md Tohid SF. Dicranopteris linearis extract inhibits the proliferation of human breast cancer cell line (MDA-MB-231) via induction of S-phase arrest and apoptosis. Pharm Biol 2018;56(1):422–432. doi:10.1080/13880209.2018.1495748, PMID:30301390.

[42] Chaudhry GE, Akim AM, Sung YY, Muhammad TST. Cancer and Apoptosis. Methods Mol Biol 2022;2543:191–210. doi:10.1007/978-1-0716-2553-8_16, PMID:36087269.

[43] Qiu J, Xiao J, Han C, Li N, Shen X, Jiang H, *et al*. Potentiation of tumor necrosis factor-alpha-induced tumor cell apoptosis by a small molecule inhibitor for anti-apoptotic protein hPEBP4. J Biol Chem 2010;285(16):12241–12247. doi:10.1074/jbc.M110.111898, PMID:20177075.

[44] Liu T, Li X, Wu M, Qin L, Chen H, Qian P. Seneca Valley Virus 2C and 3C(pro) Induce Apoptosis via Mitochondrion-Mediated Intrinsic Pathway. Front Microbiol 2019;10:1202. doi:10.3389/fmicb.2019.01202, PMID:31191506.

[45] Keshavarz M, Nejad ASM, Esghaei M, Bokharaei-Salim F, Dianat-Moghadam H, Keyvani H, *et al*. Oncolytic Newcastle disease virus reduces growth of cervical cancer cell by inducing apoptosis. Saudi J Biol Sci 2020;27(1):47–52. doi:10.1016/j.sjbs.2019.04.015, PMID:31889816.

[46] Garant KA, Shmulevitz M, Pan L, Daigle RM, Ahn DG, Gujar SA, *et al*. Oncolytic reovirus induces intracellular redistribution of Ras to promote apoptosis and progeny virus release. Oncogene 2016;35(6):771–782. doi:10.1038/onc.2015.136, PMID:25961930.

[47] Gaddy DF, Lyles DS. Oncolytic vesicular stomatitis virus induces apoptosis via signaling through PKR, Fas, and Daxx. J Virol 2007;81(6):2792–2804. doi:10.1128/JVI.01760-06, PMID:17192316.

[48] Reddy PS, Burroughs KD, Hales LM, Ganesh S, Jones BH, Idamakanti N, *et al*. Seneca Valley virus, a systemically deliverable oncolytic picornavirus, and the treatment of neuroendocrine cancers. J Natl Cancer Inst 2007;99(21):1623–1633. doi:10.1093/jnci/djm198, PMID:17971529.

[49] Rudin CM, Poirier JT, Senzer NN, Stephenson J Jr, Loesch D, Burroughs KD, *et al*. Phase I clinical study of Seneca Valley Virus (SVV-001), a replication-competent picornavirus, in advanced solid tumors with neuroendocrine features. Clin Cancer Res 2011;17(4):888–895. doi:10.1158/1078-0432.CCR-10-1706, PMID:21304001.